A Knowledge-guided Active Model Method of Skull Segmentation on T1-weighted MR images

Zuyao Y. Shan[*a], Chia-Ho Hua[b], Qing Ji[a], Carlos Parra[a], Xiaofei Ying[b], Matthew J. Krasin[b], Thomas E. Merchant[b], Larry E. Kun[b], Wilburn E. Reddick[a]

[a]Division of Translational Imaging Research, [b]Division of Radiation Oncology, Department of Radiological Sciences, St. Jude Children's Research Hospital, Memphis, Tennessee 38105, USA

ABSTRACT

Skull is the anatomic landmark for patient set up of head radiation therapy. Skull is generally segmented from CT images because CT provides better definition of skull than MR imaging. In the mean time, radiation therapy is planned on MR images for soft tissue information. This study utilized a knowledge-guided active model (KAM) method to segmented skull on MR images in order to enable radiation therapy planning with MR images as the primary planning dataset. KAM utilized age-specific skull mesh models that segmented from CT images using a conditional region growing algorithm. Skull models were transformed to given MR images using an affine registration algorithm based on normalized mutual information. The transformed mesh models actively located skull boundaries by minimizing their total energy. The preliminary validation was performed on MR and CT images from five patients. The KAM segmented skulls were compared with those segmented from CT images. The average image similarity (kappa index) was 0.57. The initial validation showed that it was promising to segment skulls directly on MR images using KAM.

Keywords: Registration, Segmentation, Mathematical Morphology

1. INTRODUCTION

Currently, radiation planning procedures use images from both CT and magnetic resonance (MR) datasets. The primary reason of including CT images is because CT provides better definition of skull than MR imaging. The skull is the key anatomic landmark for patient set up in head radiation planning procedures. However, CT does not provide good contrast in soft tissue. Furthermore, MR images exhibit better disease regions (soft tissue tumors for most patients who require head radiation therapy) than those seen on CT images. Therefore, the state of the art for radiation planning is to register images from CT and MR together. The purpose of this study was to segment skull on MR images in order to enable radiation therapy planning using MR images as the primary planning dataset. The advantages of MR-only radiation therapy simulation include (1) reducing radiation exposure for pediatric patients, (2) removing uncertainty introduced by CT and MR registration for soft tissue tumors, and (3) performing MR imaging in treatment position at the time of MR simulation. One major problem encountered toward implementing MR simulation is the lack of strong MR intensity of skull and clear differentiation of bone and air on the MR images. It is challenging to generate a good quality MR digital reconstructed radiographs showing skeletal position for treatment portal verification. Therefore, we proposed a knowledge-guided active model (KAM) method to extract skulls from MR images for this purpose.

Although there are numerous MR segmentation methods in the literature, few studies devoted to segmentation of skull because of obscure differentiation of bone and air on MR images. Several previous studies did provide segmentation of skull as a by-product. For an example, a Markov random field (MRF) approach was developed to segment MR head images into gray matter, white matter, cerebrospinal fluid, scalp-bone, and background[1]. However, because the method was not developed for skull segmentation, it does not always generate continuous bounding contours of skulls. With the development of magnetoencephalography(MEG) and electroencephalography(EEG) techniques, skull segmentation on MR images attracted some research interests recently. The impetus came from the fact that MEG and EEG inverse problems require realistic models of head for use in accurate computation of the mapping from neural current sources to scalp potentials and extracranial magnetic fields[1]. Dogdas et al. utilized Brain Surface Extractor (BET) algorithms followed by a combination of thresholding and morphological operations to

---

* zuyao.shan@stjude.org; phone 1 901 495-2673; fax 1 901 495-4398; http://www.stjude.org/shan.

segment the skull on MR images[2]. This study also did the quantitative validation using coregistered MR-CT data to evaluate their results. The average dice coefficient between automated segmented skulls and skulls from CT is 0.75. Other methods of segmentation of skull for this purpose were also reported previously. Since these studies have been reviewed in the previous report[2], we did not described them one by one here. Because forward modeling calculation in MEG and EEG are primarily affected by the upper scalp and skull, furthermore, skull morphology in the lower portion of the head is extreme complex, these methods are unreliable on skull in the lower portion of head. However, these parts of skull are generally included as landmarks in radiation therapy planning procedures.

In this paper, we described a knowledge-guided active mesh model method to segment skull on T1-weighted MR images. The skull was first extracted from CT images based on grey level intensity thresholding. A triangular mesh model was then constructed based on surface curvature from this skull and transformed onto MR images of given patient using an affine registration. The mesh model was further actively slithering to locate the boundary of skull using active mesh method. Finally, the KAM defined skull was compared with the skull from registered CT image to evaluate accuracy.

2. METHODOLOGY

2.1. Data

The MR and CT images of six patients that used for radiation therapy panning previously were retrieved for this study. The retrospectively using of the data was approved by the Institutional Review Board at St Jude Children's Research Hospital. The patients were from 9-10 years old when these images were collected. These clinic images have various voxel sizes, dimensions, and sizes of region of interest (ROI). We performed a preprocessing step to resample all CT and MR images with voxel size of $1 \times 1 \times 1$mm and similar ROIs.

2.2. Skull mesh model

The CT images from one of these six patients were randomly selected to construct the skull model. The skull was segmented from the CT images using a region growing algorithm with a threshold of bone intensity value (grey level of 1200 in this study). The triangle mesh model for the skull was constructed as follows. First, boundary surfaces of the skull including outer and inner boundaries were extracted using a 26 neighborhood judgment. Second, boundary surfaces were simplified based on the surface. Surfaces with higher curvature were simplified with more reference points and lower curvature surfaces with less reference points. Finally, a 3D triangular mesh model for the skull was constructed by triangulation of the reference points for the skull surface (Figure 1).

2.3. Knowledge guided active model (KAM)

The KAM used an object function similar to Gibbs free energy in classic physics:

$$G = H - S \tag{1}$$

Entropy (S) is the same as the normalized mutual information (NMI) described in previous studies[3]. The entropy (S) was maximized using an affine registration. To maximize the entropy, the model CT images were registered to individual MR images. Then the skull model was transformed using the transformation matrix found in the registration. The enthalpy (*H*) was minimized using active mesh method. The enthalpy includes the internal energy that controls smoothness and elasticity and the external energy that locates the image edges:

$$H = E_{ex} + E_{in} \tag{2}$$

The external energy for active model is defined by the distance of each triangle vertex to the edge of the image:

$$E_{ex} = \alpha \sum_i -\exp\left[-d(i)^2\right] \tag{3}$$

The internal energy is defined as the sum of the curvature energy *(Ecur)* and the continuity energy (*Econ*):

$$E_{cur} = \beta \sum_i \left[\frac{\sum_j s_{ij} \left(1 - \vec{n}_{ij} \bullet \vec{n}_i\right)^2}{\sum_j S_{ij}} \right], \qquad E_{cont} = \gamma \sum_i \sum_j \left(d_{ij} - \tilde{d}_i\right)^2 \tag{4}$$
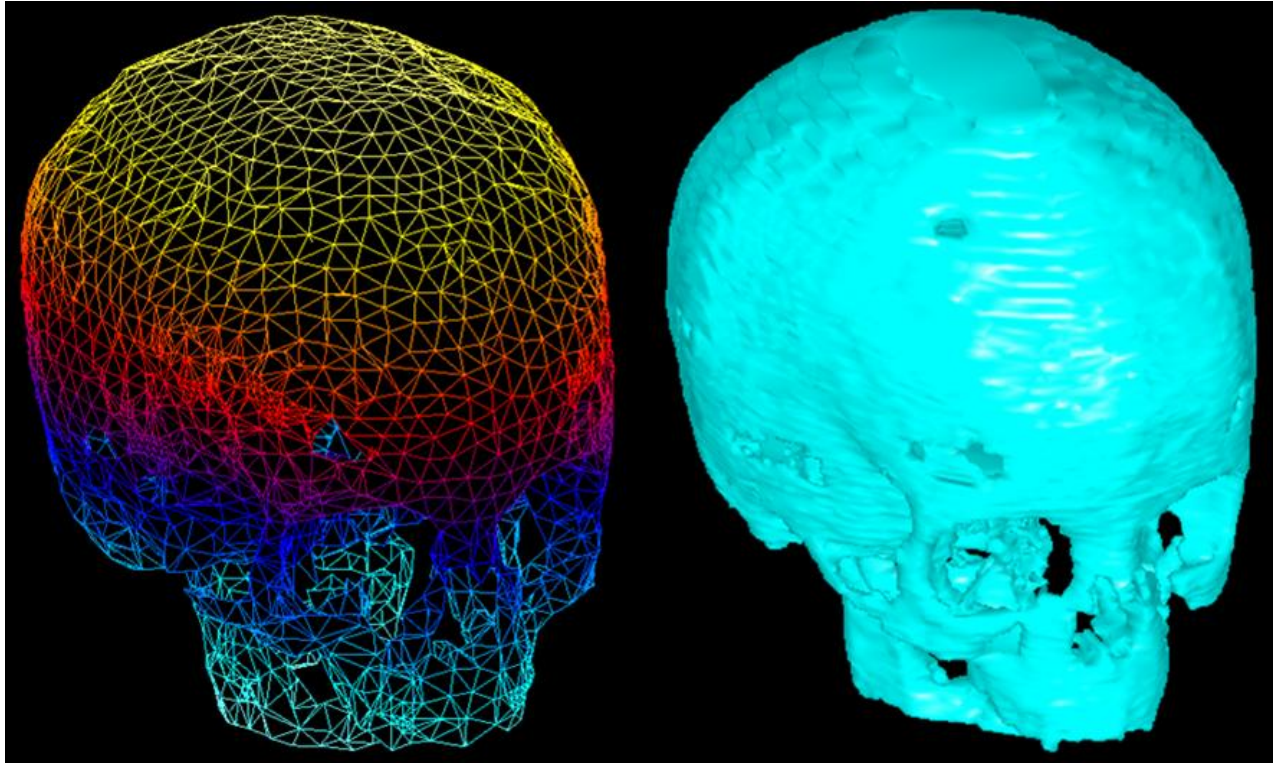
Figure 1: The skull model. The triangle mesh model was illustrated on the left and the surface rendering of the skull model was illustrated on the right. Both inner and outer surfaces of the skull were simplified by the triangle meshes based on curvature. The color from blue to red on the triangle mesh model represented the level from superior to inferior of the skull.

2.4. Validation

Five patients, excluding the one used to generate the skull model, were included in the validation study. We used the skull volumes segmented from corresponded CT images to evaluate the accuracy of the segmentation results. The CT images were registered to the MR images of the same patient. The skull was segmented from the CT images using a conditionally region growing algorithm and served as the gold standard. The KAM segmented skulls were compared with skulls segmented from CT images. The similarities between these two sets of images were evaluated by calculation of kappa index:

$$\kappa(S_a, S_b) \quad = \quad \frac{2|S_a \quad \cap \quad S_b|}{|S_a| \quad + \quad |S_b|} \tag{5}$$

where S_a refers to the skulls defined by the mesh models and S_b refers to the skull segmented from CT images.

3. RESULTS

The skull segmentation required 4 hours on a SGI Origin 300 computer without optimization of computation algorithms. Figure 2 illustrated a surface rendering of segmented skull and skull segmented based on CT from the same subject. The KAM segmented skull looks identical to skull generated from CT although parts of skull bone near eyes were missing and the surface of KAM segmented was rough than the ones segmented from CT images. Figures 3 illustrated a segmented skull overlaid back to MR and CT images. We did observe some mismatches between skull segmented by KAM and from CT images. However, overall visual inspection showed that the segmented skull agreed with skull on CT images well. Routinely used anatomical landmarks for patient setup verification such as Sella Turcica and occipital bone were easily visible.

Average kappa index between the KAM segmented skull and skull segmented from CT for five patients was 0.57.
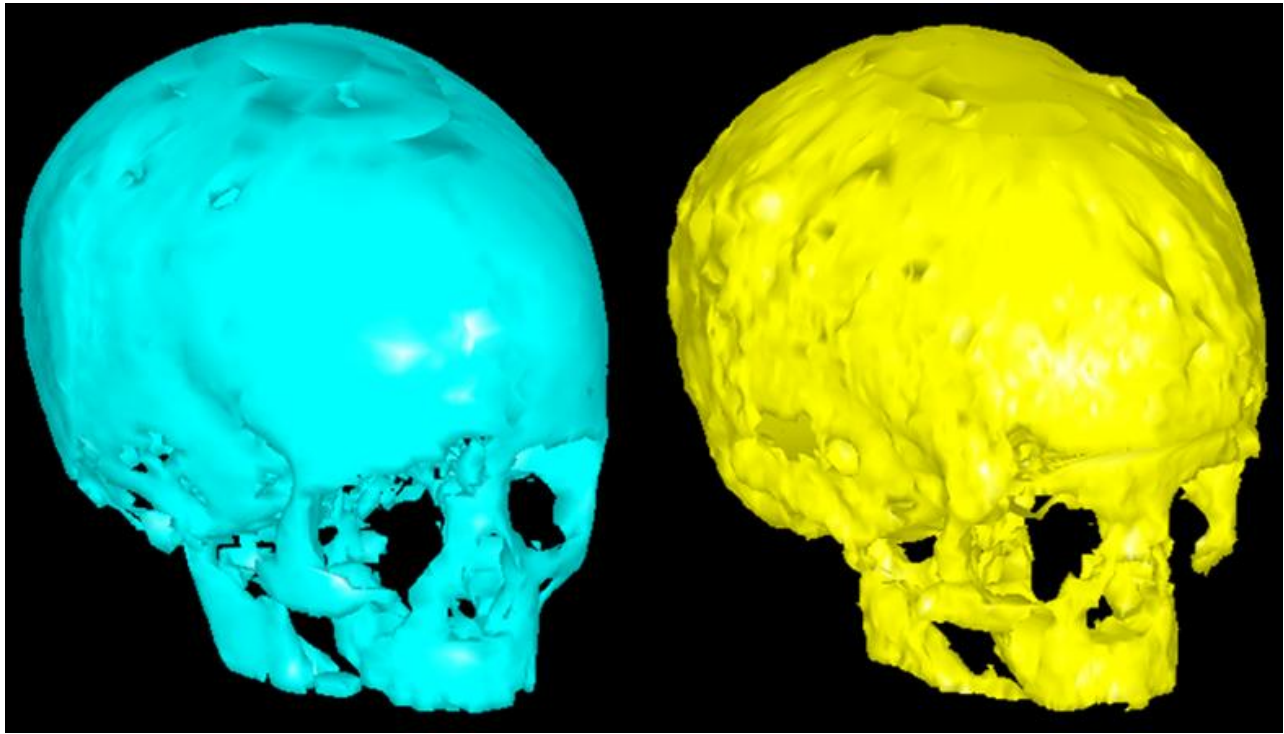
Figure 2: Surface rendering of segmented skull. The figure on the left showed a surface rendering of skull in cyan from the CT images. The figure on the right showed a surface rendering of skull segmented using KAM based on MR images from the same patients. The general shape and size of these two skulls are very similar, however, surface of skull segmented by KAM on MR images (yellow) is more rough than that from CT images.

4. DISCUSSION

We have presented a novel method, KAM, to segment the skull on MR images. To the best of our knowledge, this is the first study to segment the whole skull on MR images. Skull is generally invisible on MR images. It becomes more challenging in region close to the eyes because there is no visible boundary between bone and air. KAM utilized a prior defined model to define boundary skull and air interfaces. In the mean time, KAM compensate for inter-patient variability by minimizing of the free Gibbs energy.

The image similarity between the KAM segmented skulls and those segmented from CT were relatively low. We believed that this is caused by two major reasons. First, the skull has a high surface to volume ratio, in other words, skull is a very thin structure. Any mismatches will lead to significant decrease of kappa index. Second, there is no perfect registration between CT and MR image. KAM identified skull based on MR images. Mismatches between CT and MR images will also lead to the decrease of the skull similarity. We selected skull segmented from CT images as the gold standard because there is no other better choice. Compared with previous study[2], the accuracy of our method is lower than what they obtained. However, only the upper part of the skull was evaluated in the previous study. Furthermore, images from normal adults were used in the previous study. We also attempted to implement the method in the previous study for a comparison. However, the downloaded free software of Brain Surface Extractor (BET) algorithms failed on most of our MR data. The reason for this could be due the fact that additional inter-subject variability is high for our data because we worked on images from children with brain tumors. Additional inter-subject variability comes from that the patients were at different developmental stages and differences in surgical removal of brain tissues.

There are several shortcomings in this study. First, the validation was performed on relatively small number of patients. We are performing more extensive validation based on the success of this preliminary study. Second, we have selected skull segmented from CT images as the gold standard. As discuss above, mismatches between CT and MR
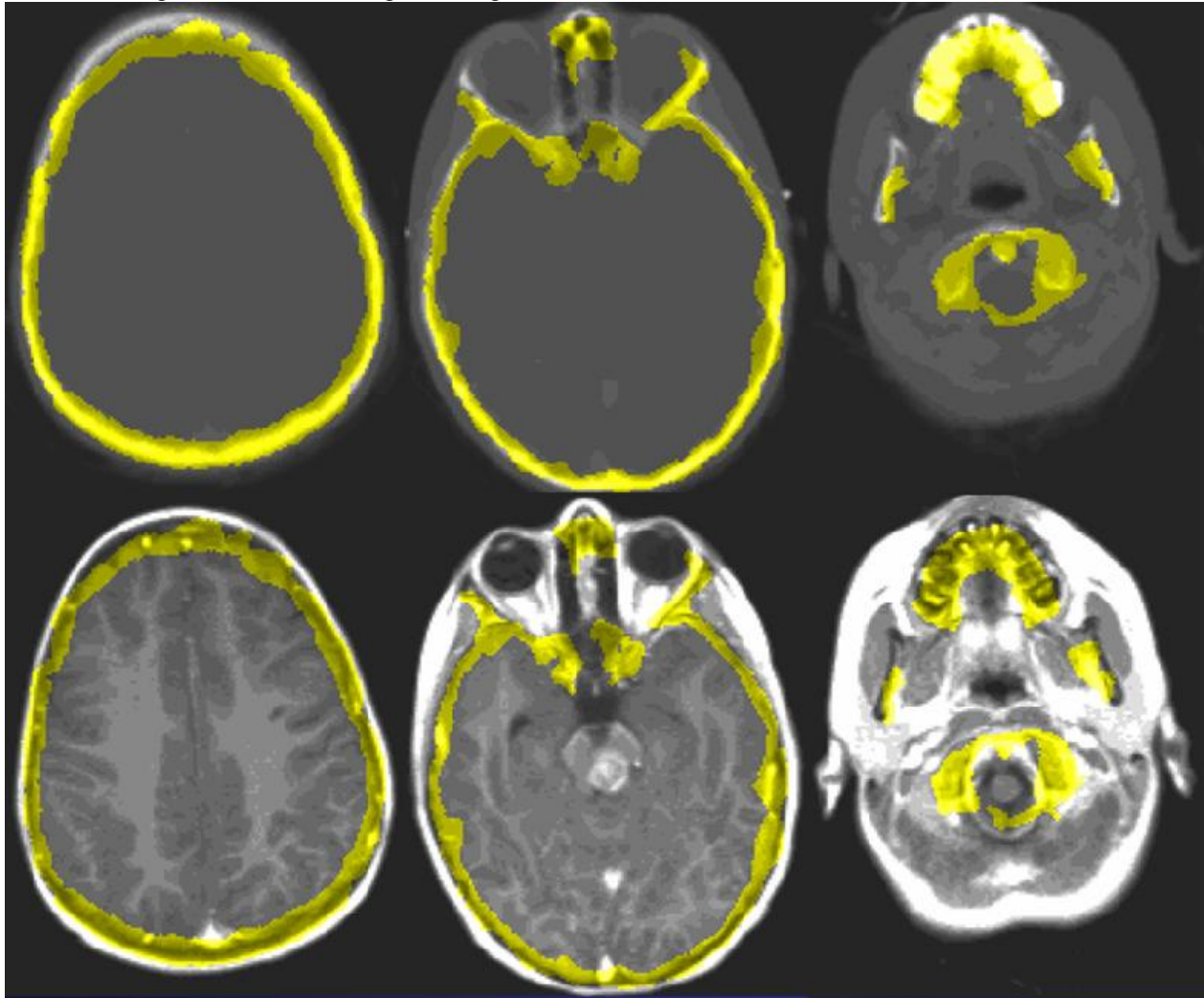
Figure 3: Illustration of skull segmented by KAM. The upper row slices are selected slices from CT images. The lower row slices are corresponded ones of MR images from the same patients. Yellow regions are segmented skull overlaid back onto the CT and MR images.

images will introduce additional discrepancies. Other validation approaches are under investigation. Finally, the accuracy of KAM segmented skull is not good enough to perform radiation therapy planning simulation yet. Some other options and improvement of the method is under investigation now.

In conclusion, we have developed a knowledge-guided active model (KAM) method to automatically segment skull from MR images with promising initial validation results

.

ACKNOWLEDGEMENTS

REFERENCES

1. K. Held, E. R. Kops, B. J. Krause, W. M. Wells, R. Kikinis, and H. W. Muller-Gartner, "Markov random field segmentation of brain MR images", *IEEE Trans. Med. Imaging* **16**, pp. 878-886, 1997.
2. B. Dogdas, D. W. Shattuck, and R. M. Leahy, "Segmentation of skull and scalp in 3-D human MRI using mathematical morphology", *Human Brain Mapping* **26**, pp. 273-285, 2005.
3. F. Maes, A. Collignon, D. Vandermeulen, G. Marchal, and P. Suetens, "Multimodality image registration by maximization of mutual information", *IEEE Trans. Med. Imaging* **16**, pp. 187-198, 1997.